Fibers and Polymers 2004, Vol.5, No.1, 59-67

Studies on Composite Filaments from Nanoclay Reinforced Polypropylene

Mangala Joshi*, M. Shaw, and B. S. Butola

Department of Textile Technology, Indian Institute of Technology, New Delhi 110016, India
(Received May 3, 2003; Revised December 30, 2003; Accepted January 6, 2004)

Abstract: The development of high tenacity, high modulus monofilaments from Polypropylene/Clay nanocomposite has been investigated. Pure sodium montmorillonite nanoclay was modified using hexadecyl trimethyl ammonium bromide (HTAB) via an ion exchange reaction. Pure and modified clay were characterized through X-ray diffraction, FTIR and TGA. The modified clay was melt blended with polypropylene (PP) in presence of a swelling agent. Composite filaments from PP/Clay nanocomposite were prepared at different weight percentages of nanoclay and the spinning and drawing conditions were optimized. The filaments were characterized for their mechanical, morphological and thermal properties. The composite PP filaments with modified clay showed improved tensile strength, modulus and reduced elongation at break. The composite filaments with unmodified clay did not show any improvement in tensile strength but the modulus improved. The sharp and narrow X-ray diffraction peaks of PP/nanoclay composite filaments indicate increase in crystallinity in presence of modified clay at small loadings (0.5 %). The improved thermal stability was observed in filaments with modified as well as unmodified clays.

Keywords: Polypropylene, Modified sodium montmorillonite nanoclay, Composite filaments, Nanocomposite

Introduction

In recent years, there has been a lot of interest in research on hybrid organic-inorganic nanocomposites [1,2]. These composites exhibit superior strength, modulus, thermal resistance and heat distortion temperature. Layered silicates (nanoclays) are one of the important nanofiller materials. The basic approach of the polymer layered silicate nanocomposites is to separate and disperse the clay platelets in polymer matrix, with dispersions ranging from simple intercalation to complete exfoliation of the silicate layers.

Polypropylene/Clay nanocomposites have been prepared by various ways. Functionalized polypropylene has been used to make PP more compatible with montmorillonite (MMT) [3-5]. Use of swelling agents (like ethylene glycol, heptane, naphtha) facilitates the intercalation of polymer chains into the interlayers [6]. In situ polymerization of propylene in presence of activated sodium montmorillonite with Ziegler - Natta catalyst leads to the formation of fully exfoliated nanocomposites [7]. Modification of MMT with compatibilizers like hexadecyl trimethyl ammonium bromide (HTAB) and octadecyl ammonium bromide to make it compatible with PP has also been reported [8]. PP/Clay nanocomposites generally show improvement in tensile strength, tensile modulus and storage modulus. They also exhibit improved thermal stability as compared to neat PP [7,9].

PP has found extensive application as a technical textile material in various engineering and high technology applications such as marine ropes, spacecrafts, sport goods, composites etc. [10]. High tenacity, high modulus polypropylene monofilaments are generally prepared by drawing polypropylene filaments at very high draw ratios, high temperatures and at very slow strain rates [11,12]. Practically there is no literature on the preparation of monofilaments from PP/MMT nanocomposites. In this study, we attempt to develop high tenacity, high modulus polypropylene filaments from PP/MMT nanocomposites.

*Corresponding author: mangala@netearth.iitd.ac.in

Experimental

Materials

The isotactic PP used was Koylene ADL (AM 120 N), a homopolymer with an MFI of 12, obtained from IPCL (India). Purified sodium montmorillonite was supplied by Kunimine Industries Co. Ltd., Japan. HTAB (Merck, AR grade) was used to modify MMT and ethylene glycol (Merck, AR grade) was used as the swelling agent. Modification of the MMT to make it more organophilic was carried out using ion exchange reaction with HTAB as per method used by earlier workers [7].

Preparation of Composite Filaments

Preparation of Master Batch

Master batches containing 10 wt% modified MMT and 10 wt% unmodified MMT in PP were prepared using Laboratory Mixing Extruder (manufactured by SDL, UK, Model No. S255). Before mixing, the MMT was swollen in ethylene glycol to help it disperse better in PP. The temperature of the rotor and die zone was kept at 180 and 210 ^{o}C respectively. The rotor speed was 45 rpm. The extruded strands were then cut using a granulator into chips.

Extrusion of Filament

The dispersion of nanoclay in PP matrix for preparation of PP/clay nanocomposite monofilaments was done by melt mixing. The mixing and extrusion of filaments was carried

Table 1. Sample composition and coding

Sample code	Composition
PP	Neat Polypropylene
M5	PP + 0.5 % Modified Clay
M10	PP + 1.0 % Modified Clay
M15	PP + 1.5 % Modified Clay
U5	PP + 0.5 % Unmodified Clay
U10	PP + 1.0 % Unmodified Clay
UC	Unmodified Clay
MC	Modified Clay

out in a laboratory model Single Screw Extruder, Betol, U. K. The melt spinning parameters i.e. screw speed, temperature at different zones in the extruder and take up speed were optimized to get a uniform filament. The temperature of I, II, III and die zones were kept at 170, 180, 200, and 225 °C respectively. The screw speed was 5 rpm and the as spun PP filaments were quenched in a water bath maintained at a temperature of 12-14 °C and collected at a take-up speed of 4 m/min. PP filaments with modified clay loading of 0.5, 1.0, 1.5, and 2.0 wt% and unmodified clay loading of 0.5 and 1.0 wt% were prepared. The filaments containing 1.5 wt% and more of unmodified clay could not be produced as the spinline was found to be unstable on account of frequent breakages of the as spun filaments. The composition of different sample batches is given in Table 1.

Drawing of Filament

Each as spun filament sample was drawn using laboratory model two zone drawing machine (fabricated) and the optimum conditions for drawing of the composite filaments were investigated. The filaments were drawn in three stages. The drawing temperatures were kept at 80, 110, and 160 °C and the draw ratios of 6.0, 1.2, and 1.8 were used in I, II, and III stages respectively. The total draw ratio was ~13.

Characterization of Unmodified and Modified MMT

Thermogravimetric Analysis (TGA)

The TGA of unmodified, modified MMT and HTAB was performed on Perkin-Elmer TGA-7 Thermogravimetric Analyzer. The temperature range was kept between 25 and 750 °C with a heating rate of 10 °C/min in nitrogen atmosphere.

FTIR Analysis

The IR spectra of the samples were recorded in KBr pellet form on Perkin-Elmer 883 Infrared Spectrometer. Separate KBr pellets were prepared with 1 % by weight of the samples (unmodified clay, modified clay and HTAB). The frequency range varied from 400 to 4400 cm^{-1} at a nominal resolution of 4 cm^{-1}. The number of scans for each spectrum was fixed at 56.

Small Angle X-ray Diffraction

The SAXS studies on modified and unmodified MMT were carried out on Bruker Axs X-ray diffractometer (D8 Advanced) using CuKα radiation operated at 40 kV and 30 mA. The data were collected in 2θ angle range 2-12 ° at a scanning rate of 0.5 °/min

Composite Filament Structure and Morphological Characterization

The nanocomposite filaments were characterized for their morphological features using XRD, optical birefringence, optical microscopy and SEM.

Sonic Modulus

Sonic modulus of the filaments was measured on the dynamic modulus tester PPM-5R made by HMM Morgan Co. It is a measure of the overall molecular orientation. Sonic modulus is calculated using the formula

$$E = \rho \times C^2 \tag{1}$$

Where E = modulus in GPa, ρ = density in g/cm^3 (ρ = 0.92 for PP), C = sonic velocity in km/sec.

Wide Angle X-ray Diffraction

WAXD studies of the samples were carried out on Philips X-ray diffractometer with Nickel-filtered CuKα as radiation source. The diffractometer was operated at 40 kV and 30 mA in reflection mode with angle 2θ range 10-35 ° at a scanning rate of 2 °/min.

Crystalline Orientation Function

WAXD studies were used to determine the crystalline orientation of melt-spun filaments. The Herman's orientation function [13] is defined as:

$$f_x = \frac{3(\cos^2\theta_{hkl,z}) - 1}{2} \tag{2}$$

where θ is angle between reference direction (filament axis) and the x-crystallographic axis (x = a, b or c). Assuming rotational symmetry about the filament axis:

$$\overline{(\cos^2\theta_{hkl,z})} = \frac{\int_0^{\pi/2} I(\theta)\cos^2\theta\sin\theta d\theta}{\int_0^{\pi/2} I(\theta)\sin\theta d\theta} \tag{3}$$

where $I(\theta)$ is the intensity of diffraction from the (hkl) planes which are normal to the x-crystallographic direction. The integrals in equation are evaluated numerically from the intensity distribution of (110) and (040) reflection planes.

For monoclinic PP,

$$f_c = \frac{3\langle\cos^2\theta_{c,z}\rangle - 1}{2} \tag{4}$$

where $\cos^2\theta_{c,z} = 1 - 1.099\cos^2\theta_{110,z} - 0.901\cos^2\theta_{040,z}$ (5)

$\cos^2\theta_{110,z}$ and $\cos^2\theta_{040,z}$ are obtained from azimuthal intensity distribution measurements of (110) and (040) reflection using the equation (3).

X-ray Crystallinity

The weight fraction crystallinity of the nanocomposite filaments was determined by superimposing the amorphous curve of PP [14] on the $I(\theta)$ vs 2θ diffraction scans obtained from the x-ray difractometer and using the following formula after segregating the crystalline contribution:

$$X_c = \frac{\int_0^{\alpha} s^2 I_c(s) ds}{\int_0^{\alpha} s^2 I_s(s) ds} \quad (6)$$

Where X_c = Crystalline mass fraction, $s = 2\sin\theta/\lambda$, I_c = Crystalline Diffraction intensity, I_s = Total Diffraction Intensity, λ= 1.54 Å, θ = Bragg's angle, α = maximum scan angle.

Optical Birefringence

The optical retardation of the filaments was measured on optical polarizing microscope manufactured by Vickers Instrument, England with Leitz Wetzler tilting plate type quartz compensator to get the birefringence values. The diameter of the filaments was measured using Leica DMLP Optical Microscope. An average of ten readings was taken for each sample. The optical birefringence of the filaments was calculated using formula:

$$\Delta n = \frac{6.18 \times phase\ difference\ (nm)}{1000 \times diameter\ (\mu m)} \quad (7)$$

Scanning Electron Microscopy

The surface and cross sectional views were observed under scanning electron microscope, Cambridge Stereoscan S-60. The samples were fractured in liquid nitrogen for cross sectional view.

Mechanical Property Evaluation

The tensile strength, tensile modulus, elongation at break and work of rupture were measured on tensile testing equipment, Statimat Me from Textechno, Germany. A gauge length of 100 mm was used and the strain rate was selected in such away so as to keep the time to break at approximately 20 ± 2 seconds. All tensile testing results reported are in terms of average of 10 readings.

Creep Studies

Creep, the time dependent property of the nanocomposite filaments was studied using a simple instrument, which consisted of a vertical wooden scale and different weights for application of load. The filaments were stressed at a stress level of 260 MPa and a gauge length of 24 cm was used. The elongation of the filaments was recorded for three hours with measurements being taken at an interval of every two minutes for the first half an hour and 30 minutes for the later part. The creep compliance was calculated and plotted as a function of time.

Results and Discussion

Characterization of Unmodified and Modified MMT

The nanoclay in its unmodified form is not dispersible in PP due to its polar nature. Therefore the clay was modified with long chain alkyl quaternary ammonium salt - HTAB by an ion exchange reaction. Modification of the clay makes it organophilic so that it can easily disperse in the PP matrix. The unmodified and modified clays were characterized using following techniques:

FTIR Spectra

The FTIR spectra of modified clay, unmodified clay and HTAB are shown in the Figure 1 and the characteristic peaks for the same are summarized in Table 2. The peaks at 3628.13 and 1633.99 cm^{-1} represent O-H groups in the silicate structure [15]. These are present in both unmodified and modified clays. The C-H stretching bands at 2922.61 and 2850.25 cm^{-1}, the N-H bending vibration at 1490 cm^{-1} and the peak at 1470.01 cm^{-1} representing C-H_2 bending is seen only in the spectra of modified clay [16]. The presence of peaks due to C-H and N-H bonds which are characteristic

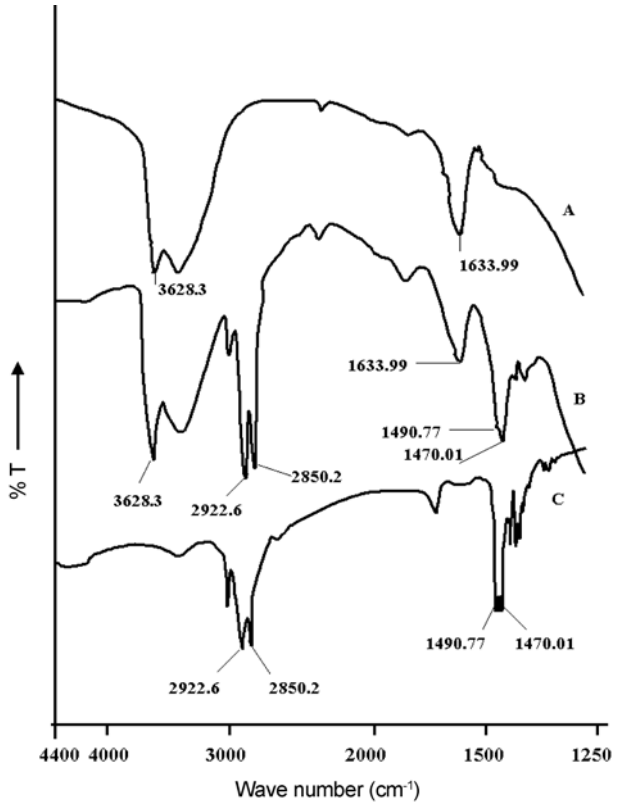

Figure 1. FTIR Spectra: A-Unmodified Clay, B-Modified Clay, C-HTAB.

Table 2. Summary of FTIR study of modified and unmodified clay

Wave number (cm^{-1})	Bond	Modified clay	Unmodified clay
3628.13	O-H	√ [a]	√
1633.99	O-H	√	√
2922.61	C-H Stretching	√	×
2850.25	C-H Stretching	√	×
1470.01	C-H_2 Bending	√	×
1490	N-H Bending	√	×

[a]: "√"-present and "×"-absent

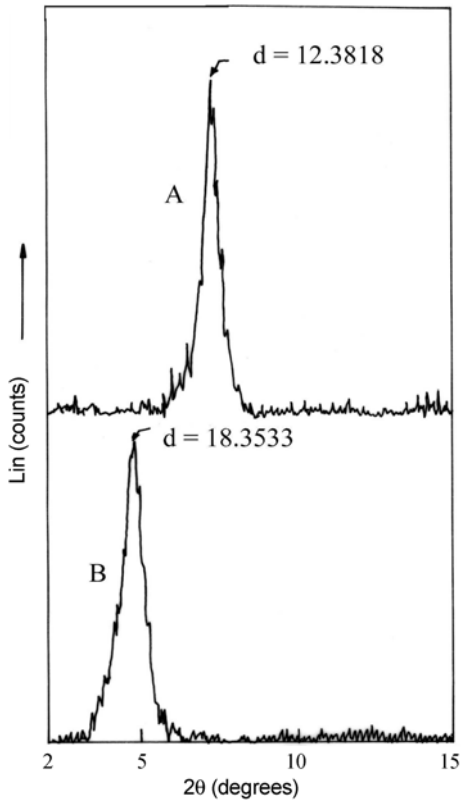

Figure 2. XRD diffractograms: A-Unmodified Clay, B-Modified Clay.

of the HTAB, in the FTIR of the modified clay confirms that the clay has been chemically modified by an ion exchange reaction with HTAB.

X-Ray Diffraction

The XRD of both unmodified and modified clay was carried out in powder form and the profiles are shown in Figure 2. The unmodified and modified clay show their characteristic diffraction peaks at 2θ angles 7.06 and 4.68 ^{o} respectively. The shifting of diffraction maxima from 7.04 to 4.68 ^{o} indicates that the d spacing of ordered clay domains has increased from 1.22 nm to 1.83 nm after modification.

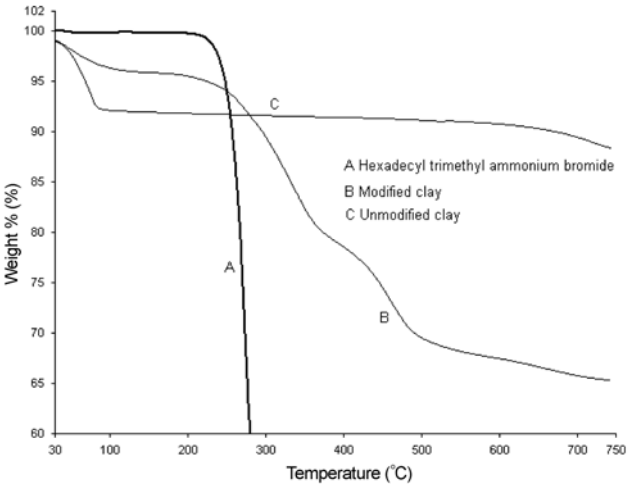

Figure 3. TGA Thermograms of HTAB, modified and unmodified clay.

The inter layer d spacing increases as the alkyl chains are tethered in the clay galleries. The increase in the basal distance 'd spacing' facilitates the intercalation of polymeric molecular chains into the inter layer galleries of the clay.

Thermogravimetric Analysis

The TGA thermograms of HTAB, unmodified MMT and modified MMT are shown in Figure 3. In the case of unmodified MMT, the initial weight loss of 6.9 % in the temperature range 30-100 ^{o}C occurs due to loss of water, which hydrates Na^{+} ions. Further weight loss between 630 and 744 ^{o}C is reported to occur due to dehydroxylation of MMT [15,16]. The dehydroxylation of O-H present in the silicate structure occurs when it is heated beyond 500 ^{o}C. In case of modified MMT, the weight loss takes place in 3 steps. A very small loss of about 3 wt% takes place between 28 and 100 ^{o}C on account of loss of water. The water loss value decreases from ~7 wt% for pure MMT to 3 wt% for modified MMT indicating reduced hydrophilic nature of modified MMT. The second weight loss (~25 %) takes place between 230 and 500 ^{o}C and is due to decomposition and oxidation of intercalated quaternary salt in two subsequent steps. The melt mixing of polypropylene and MMT was carried out at 225 ^{o}C, so no significant decomposition of the intercalated quaternary salt is expected at this temperature.

Spinning

PP/Clay nanocomposite filaments were prepared as per details given in the experimental section. While with modified MMT the filaments could be spun successfully up to 2 % by weight, in case of unmodified MMT they could not be spun beyond 1.0 wt% as spin line was found to be unstable leading to frequent breakages. Although the presence of clay in PP adversely affects its spinning performance as presence of any foreign material in a fibre forming polymer changes

its rheological properties, it is clear that modification of MMT clay with HTAB helps in dispersing MMT better in PP matrix (as compared to unmodified MMT) and thus improves the spinnability of PP/Clay nanocomposite.

Drawing

All the PP/clay nanocomposite and neat PP filaments were drawn to a draw ratio of 13 as per details given in the experimental section. The drawability of synthetic fibres depends on the initial morphology of as spun filaments, which influences its structure and properties. PP Filaments under applied tensile stress mostly form α crystalline structure when quenched in air and smectic crystalline structure when quenched in ice-cold water [11]. When the as spun filaments come out of the extruder, the crystallization takes place by two mechanisms. One is stress-induced crystallization and the other is heterogeneous crystallization. At higher take up speeds the stress-induced crystallization dominates while the lower take up speeds favor heterogeneous crystallization. In case of quiescent crystallization, neat PP forms α crystallites at low cooling rates and mesomorphic smectic crystallites at higher cooling rates in presence of montmorillonite [17]. The as spun composite filaments would be containing both α and smectic crystalline forms, the composition of which is determined by the actual cooling rate. PP with less stable pseudo crystalline smectic structure can be drawn to a higher degree than one with more stable α-crystalline form. Hence the extruded filaments were quenched in ice-cold water to facilitate the formation of smectic structure. The drawability of this smectic structure is maximum at 60 °C [18], hence the filaments were initially drawn at a temperature of 60 °C in the first drawing zone but showed multiple necking and whitening (indication of void formation due to overdrawing). The temperature and strain rate are important parameters to control these two drawbacks. The stain rate was kept constant and temperature was gradually increased. Stable neck was formed when the temperature was raised to 80 °C. At low speed of extrusion as used here, heterogeneous crystallization along with stress induced crystallization influences the morphology of the filaments. The heterogeneous crystallization due to the presence of clay in as spun composite filaments leads to increase in crystallinity as compared to the neat PP filaments, making it more difficult to draw composite filaments as compared to the neat PP filaments and hence the need for higher drawing temperature (~80 °C). After the first stage drawing, the filaments develop crystallinity and their drawability reduces, hence higher drawing temperature (110 °C) and lower draw ratio were used in the second stage drawing. The filaments were drawn at 160 ºC in the third stage. The higher drawing temperature of 160 ºC in the third zone initiates partial melting and recrystallization of imperfect and smaller crystals leading to perfection of crystals.

Characterization of PP/nanoclay Composite Filaments

Morphological Characterization

The structural and morphological characterization of PP/nanoclay reinforced composite filaments was done using wide angle X-ray, DSC, sonic modulus and birefringence.

Wide Angle X-ray Diffraction

The X-ray difractograms of PP, M5, and U5 are shown in Figure 4. The diffraction peaks at (110), (040) and (111) planes are sharper in composite filaments as compared to corresponding peaks in neat PP. The narrowing down of the peaks is associated with perfection of crystals. The X-ray crystallinity values of drawn PP/nanoclay composite filaments are given in the Table 3.

It is observed that the crystallinity has significantly increased in composite filaments with lower weight percentage of modified MMT i.e., 0.5 wt% compared to neat PP whereas at higher weight percentages, the crystallinity decreases. The

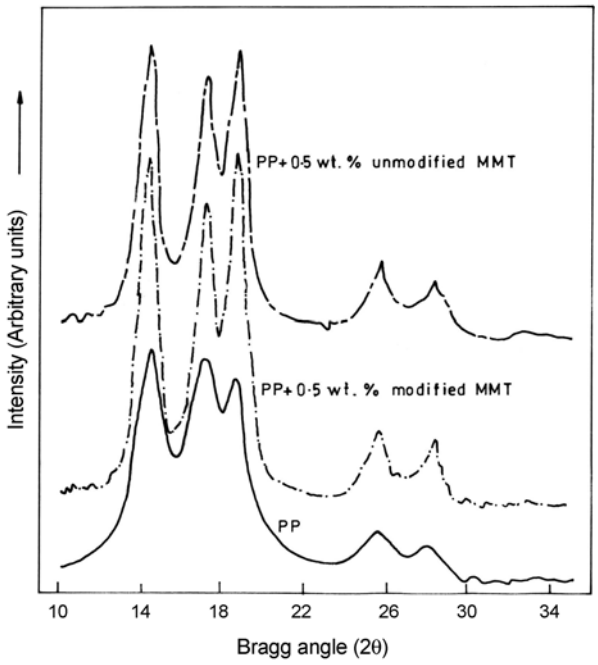

Figure 4. XRD Diffractograms of PP/clay nanocomposite filaments.

Table 3. X-Ray crystallinity of composite filaments

Sample code	XRD crystallinity (%)
PP	62
M5	69
M10	60
M15	50
U5	56
U10	58

Table 4. Crystalline orientation function, Birefringence and sonic modulus of composite filaments

Sample code	Crystalline orientation	Birefringence	Sonic modulus (GPa)
PP	0.87	0.035	30.5
M5	0.89	0.028	25.5
U5	0.79	0.025	24.0

composite filaments from unmodified MMT at 0.5 and 1.0 wt% show lower values as compared to modified MMT composites. This may be due to modified MMT being better dispersed in PP matrix at lower concentration of 0.5 wt%, and hence not interfering in the crystallization process. The crystalline orientation function was calculated using equation (5) and the values are given in the Table 4. The crystalline orientation function, which depends on the spin line stress, is unaltered in case of nanocomposites having 0.5 wt% modified MMT (M5) and decreases slightly in case of nanocomposites with 0.5 wt % unmodified MMT (U5).

Birefringence

Birefringence measures the overall (amorphous and crystalline) molecular orientation of the polymer chains. The birefringence values for the various composite filaments are given in Table 4. The birefringence values for composite filaments with both modified and unmodified clays are lower than those for neat PP. This may be due to the presence of rigid clay particles in PP matrix, which restrict orientation of PP chains during drawing. This trend is also supported by the sonic modulus values for the composite filaments.

Sonic Modulus

The sonic modulus of all the filament samples was determined and is given in Table 4. Although the sonic modulus values of composite filaments are lower than those for neat PP filaments, there is not much difference in the sonic modulus values of different composite filaments. The presence of clay (modified and unmodified) in the polymer melt disturbs molecular orientation of the chains, which is also evident from the birefringence values of composite filaments, which are lower than those for neat PP filaments. The molecular orientation is disturbed more in case of unmodified clay, which is less homogeneously dispersed and forms micro size clay agglomerates dispersed in the matrix.

Mechanical Properties

The mechanical properties of the filaments such as tensile strength, tensile modulus and elongation are given in Table 5 and the stress-strain curves shown in Figure 5. It is observed that there is a significant improvement in the modulus and the breaking stress of the modified clay composite filaments even at very low weight fractions of clay (~0.5-1.0 wt%) as compared to neat PP filaments. The breaking stress of the

Table 5. Tensile properties of composite filaments

Sample code	Breaking stress (MPa)	Breaking elongation (%)	Modulus at 1% elongation (GPa)	Modulus at 5 % elongation (GPa)
PP	532	19.7	7.6	5.13
M5	690	7.2	15.0	11.0
M10	642	6.6	15.5	10.8
M15	432	12.2	7.1	5.0
U5	525	7.6	11	7.9
U10	421	5.2	9.5	5.3

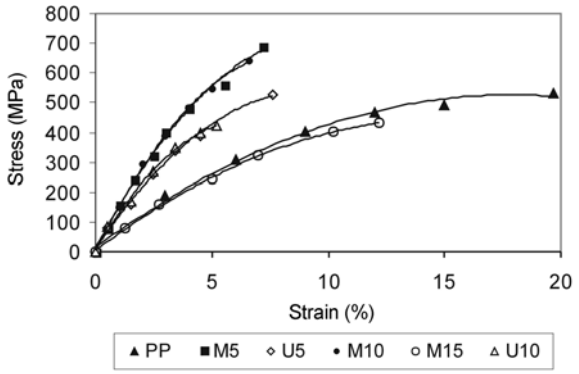

Figure 5. Stress-strain curves of PP/clay nanocomposite filaments.

composite filaments with modified clay at 0.5 and 1.0 wt% (M5, M10) increases by up to 30 % as compared to neat PP filaments. As the loading of modified clay increases in the PP matrix, the increase in the breaking stress starts decreasing and at 1.5 wt% of clay it is actually lower than neat PP. The enhancement in mechanical properties can be explained on the basis of modified clay platelets reinforcing the PP matrix at nanolevel due to nanodispersion resulting in combination of intercalated and exfoliated structure. The formation of intercalated/exfoliated structure is favored at higher temperature where the rate of crystallization is lower and the chain mobility is high. Under such conditions polymer chains can diffuse into the interlayers of the clays [19]. The processing of composite filaments (which were extruded at fairly high temperature i.e. 225 ^{o}C and drawn at 160 ^{o}C in final stage) may have favored the process of intercalation and exfoliation of clays in the PP matrix. The specific surface area of dispersed clay increases with decrease in the particle size. This results in increase in the volume fraction of the interfacial regions and helps in better stress transfer. It is reported that increase in the volume fraction of the interfacial regions in case of nanocomposites leads to increase in the tensile strength [20]. The modulus of composite filaments also shows significant increase (almost doubles with 0.5 and 1.0 wt% of modified MMT), whereas the percentage elongation at break shows a sharp decrease. This trend is in line with increase in stiffness as well as brittleness in composite materials on addition of reinforcing fillers [21]. However, with unmodified

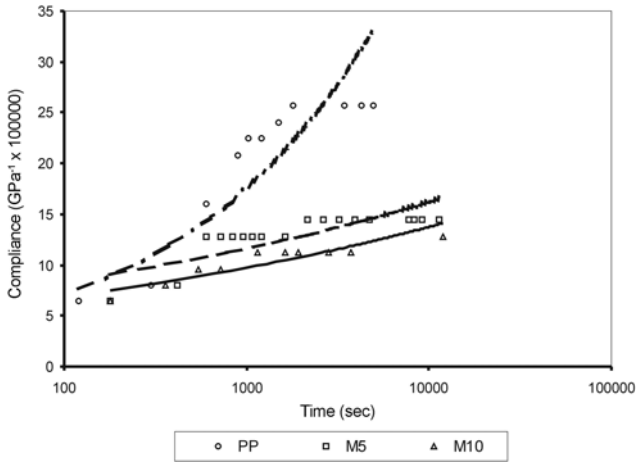

Figure 6. Creep compliance vs time plots of PP/clay nanocomposite filaments.

Table 6. Data on creep behavior of composite filaments at (stress 260 MPa)

Sample code	Extension % after 3 min	Extension % after 3 hrs
PP	1.67	8.3
M5	1.67	3.75
M10	1.67	3.33

clay the breaking strength and breaking elongation is reduced at similar clay loadings as compared to the neat PP filaments, indicating that unmodified clay was unable to disperse at nanolevel, forming microsized aggregates of clay particles dispersed in PP matrix and hence could not reinforce the polymer.

Creep Studies

The creep compliance of filaments is plotted with log time under loading stress of 260 MPa, which is equal to the 50 % of the breaking stress level of the neat and composite filaments. The variation of creep compliance with time is shown in Figure 6. It is observed that the creep compliance of PP filament increases with time at a much higher rate as compared to composite filaments indicating better resistance to creep for composite filaments. Table 6 shows the elongation percentage at different times of loading. While the extension just after loading (within 3 min) is same in all the cases, the extension after 3 hours is considerably lower in case of composite filaments as compared to neat PP filaments. The increased crystallinity and restricted mobility of the chains due to intercalation and reinforcement of the polypropylene chains by clay may be the reasons for improvement in the creep resistance of composite filaments.

Thermal Properties

The thermal resistance of the composite and neat PP

Table 7. Data from TGA analysis of filaments

Sample code	Onset temperature (°C)	Inflection peak (°C)
PP	338	446
M5	368	474
M10	370	478
U5	374	387
U10	372	486

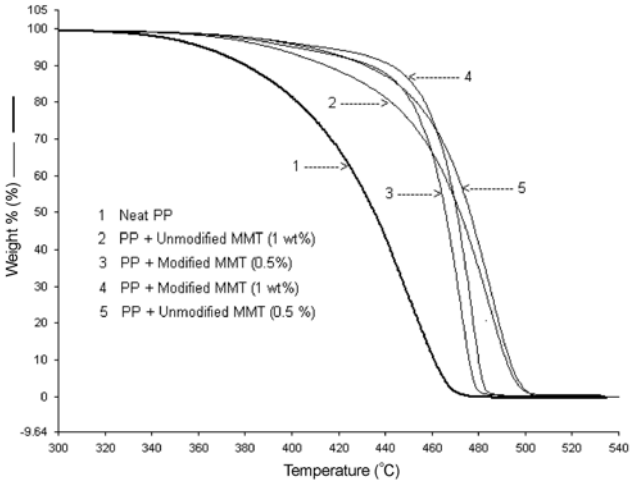

Figure 7. TGA thermograms of PP/clay nanocomposite filaments.

filaments was studied using Thermogravimetric analysis (TGA). The results are given in the Table 7 and thermograms in Figure 7. It is clear that the composite filaments with both modified and unmodified MMT have increased thermal resistance and the onset temperature of degradation increases by approximately 30 °C over neat PP at 0.5 and 1.0 wt% clay loadings. Since clay is itself a thermally resistant material, it imparts improved thermal stability to the composite filaments. In nanocomposites, high thermal resistance is also attributed to thin char formation, which does not fracture as the uniformly dispersed clay platelets reinforce the char structure [1,2].

SEM

The Scanning Electron microscopic (SEM) images of surface and cross-sections of composite filaments are shown in Figure 8. The cross sectional view of PP/modified MMT (M5) composite filament (Figure 8(a)) clearly shows that the clay is evenly dispersed in the PP matrix and the dispersed clay particles are in the range of 100-500 nm in diameter. Ideally, the particle size of the dispersed phase should be below 100 nm for a composite to be called a true nanocomposite. However, since the composite filaments with modified MMT show reinforcement, it can be postulated that intercalation of clay has taken place and smaller clay particles (<100 nm) are also present which may be too small to be resolved at the given magnification. The presence of few bigger size particles (500 nm)

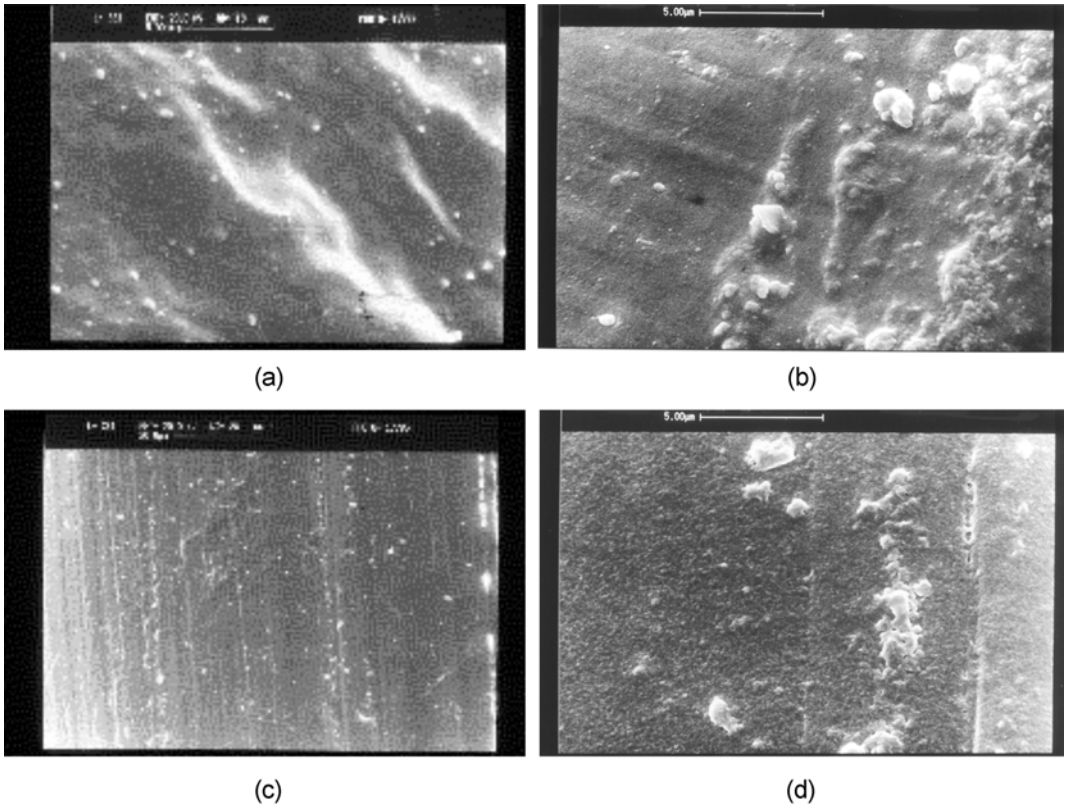

Figure 8. SEM micrographs: (a) Cross sectional view of 0.5 wt% of modified clay/PP filament (M5), (b) Cross sectional view of 0.5 wt% of unmodified clay/PP filament (U5), (c) Surface view of 0.5 wt% of modified clay/PP filament (M5), (d) Surface view of 0.5 wt% of unmodified clay/PP filament (U5).

can be explained on the basis of lack of high shear during melt mixing in the single screw extruder. Typically, twin-screw extruders are used for providing high shear and intensive mixing conditions for proper dispersion of nanomaterials in polymeric matrices in melt intercalation techniques. The presence of clay leads to fibrillation in composite filaments as seen in the surface view micrographs (Figure 8(c) and 8(d)). From SEM image of cross section of PP/unmodified MMT (U5) composite filament (Figure 8(b)), it is observed that unmodified clay particles are not uniformly dispersed in the PP matrix and tend to agglomerate as is evident from the micrographs. Also, the size of clay particles is much larger (1-2 microns) than those in PP/modified MMT composite filament. The polar nature of unmodified MMT is the primary reason for the incompatibility between hydrophilic unmodified clay and hydrophobic PP, which results in poor properties of PP/ unmodified MMT composite filaments as compared to neat PP filaments.

Conclusion

Nanoclay reinforced PP nanocomposites could be spun and drawn successfully for 0.5, 1.0, and 1.5 wt% of the modified clay loading. Beyond 1.5 wt% the spinnability was poor. The 0.5 and 1.0 wt% reinforced PP/modified nanoclay composite filaments show significant increase in tenacity (~30 %) as well as modulus (~100 %) as compared to neat PP filaments. The modified clay content in the range of 0.5-1.0 wt% gives optimum properties. The composite filaments also show improved creep resistance and thermal stability as compared to neat PP filaments. The XRD of the samples showed enhanced crystallinity in presence of modified clay. The SEM studies indicate good dispersion of modified clay in the PP. The modification of MMT using HTAB increases the interlayer d-spacing from 1.22 to 1.83 nm as is evident from the XRD data. This has facilitated the homogeneous dispersion of clay in PP matrix forming a combination of intercalated and exfoliated structure, responsible for enhanced mechanical and thermal properties. However, true molecular dispersion resulting in a completely intercalated/exfoliated composite structure is expected through the use of twin-screw extruder for intensive melt mixing and suitable compatibilizers, which is under investigation.

References

1. E. P. Giannelis, R. Krishnamoorti, and E. Manias, *Advances in Polymer Science*, **138**, 107 (1999).

2. M. Alexander and P. Dubois, *Materials Science and Engineering*, **28**, 1 (2000).
3. M. Kato, A. Usuki, and A. Okada, *J. Applied Polymer Science*, **66**, 1781 (1997).
4. M. Kawasumi, N. Hasegawa, M. Kato, A. Usuki, and A. Okada, *Macromolecules*, **30**, 6333 (1997).
5. N. Hasegawa, M. Kawasumi, M. Kato, A. Usuki, and A. Okada, *J. Applied Polymer Science*, **67**, 87 (1998).
6. D. Wolf, A. Fuchs, U. Wagenknecht, B. Kretzchmar, D. Jehnichen, and L. Haussler, *Proc. Eurofiller99*, *Lyon-Villeurbanne*, 6-9 September (1999).
7. M. Jisheng, Z. Qi, and Y. Hu, *J. Applied Polymer Science*, **82**, 3611 (2001).
8. Y. Tang, Y. Hu, L. Song, R. Zong, Z. Gui, Z. Chen, and W. Fan, *Polymer Degradation and Stability,* **82**, 127 (2003).
9. J. W. Gilman, C. L. Jackson, A. B. Morgan, R. Harris, E. Manias, E. P. Giannelis, M. Wuthenow, D. Hilton, and S. H. Philips, *Chemistry of Materials*, **12**, 1866 (2000).
10. V. B. Gupta and V. K. Kothari, "Manufactured Fibre Technology", 1st ed., p.457 Chapman & Hall, London, 1997.
11. E. Andreeassen, O. J. Myhr, L. Hinrichsen, and K. Gostad, *J. Applied Polymer Science*, **52**, 1505 (1994).
12. R. J. Sammuel, "Structured Polymer Properties", 1st ed., p.210, Wiley, New York, 1973.
13. L. E. Alexander, "X-Ray Diffraction", Freeman, San Francisco, 1963.
14. R. P. Runt, "Encyclopedia of Polymer Science and Engineering", 2nd ed. (H. F. Mark, N. M. Bikales, C. G. Overberger, and G. Menger Eds.), Vol. 4, p.482, Wiley-Inter science, New York, 1986.
15. X. Z. Wei and Z Gao, *Thermochimica Acta*, **367**, 339 (2001).
16. P. Bala, B. K. Samantaray, and S. K. Srivastava, *Material Research Bulletin*, **35**, 1717 (2000).
17. H. Wang, C. Zeng, M. Elkovitch, and L. J. Lee, *Polymer Engineering and Science*, **41**, 2036 (2001).
18. I. C. Wang, M. G. Dobb, and J. G. Tomka, *J. Textile Institute*, **86**, 383 (1995).
19. P. Maiti, H. P. Nam, and M. Okamoto, *Macromolecules*, **35**, 2042 (2002).
20. X. L. Ji, J. K. Jing, W. Jiyang, and B. Z. Jiang, *Polymer Engineering and Science*, **42**, 983 (2002).
21. A. Ahmed and F. R. Jones, *J. of Material Science*, **25**, 4933 (1990).